Experimental and numerical study of heat and mass transfer during contact heating of sliced potatoes

T. Viné, D. Flick, E. Bernuau, B. Broyart

Experimental and numerical study of heat and mass transfer during contact heating of sliced potatoes

Viné, T.[a,b], Flick, D.[a,b], Bernuau, E[a,b], Broyart, B.[a,b,1]

[a] AgroParisTech, UMR1145 Joint Research Unit for Food Process Engineering, 91300 Massy, France

[b] INRA, UMR1145 Joint Research Unit for Food Process Engineering, 91300 Massy, France

Abstract

Studies concerning the contact heating of food products remain relatively rare in the literature despite the importance of this mode of heat transfer in many operations (grilling, pan-frying). To deal with this, kinetics of product water loss and temperature rise were recorded during contact heating of potato slices in order to examine the influence of the heating power and of the presence or not of an oil layer below the heated product. From the experimental data acquired, a 2D mathematical model based on a moving boiling-front approach was developed and validated allowing the determination of contact heat transfer coefficient values of 512.2 ± 12.4 $W.m^{-2}.K^{-1}$ and 197.5 ± 5.8 $W.m^{-2}.K^{-1}$ for experiments with and without oil respectively. The analysis of the simulation results showed that the overall heating of the product is limited by: (i) the evaporation of liquid water at the location of a boiling front propagating within the heated product and (ii) by the development of a dried region (crust) in the lower part of the product acting as a thermal insulating layer. It should also be noted that

[1] Corresponding author: bertrand.broyart@agroparistech.fr

25 the determination of the contact heat transfer coefficient can become an incidental problem
26 (especially for experiments with oil) since the thermal contact resistance is often much lower
27 than the thermal resistance associated with conduction in the dried region of the product.

Nomenclature

Symbol	Definition	Units
a_w	Water activity	-
Cp	Specific heat capacity	$\mathrm{J.kg^{-1}.K^{-1}}$
D_w	Apparent water diffusivity	$\mathrm{m^2.s^{-1}}$
e_{cr}	Crust thickness	m
h	Heat transfer coefficient	$\mathrm{W.m^{-2}.K^{-1}}$
$\hat{H}$	Enthalpy (by unit-mass of dry matter)	$\mathrm{J.kg^{-1}}$
$\dot{H}$	Enthalpy flux	$\mathrm{W.m^{-2}}$
k	External mass transfer coefficient	$\mathrm{m.s^{-1}}$
Le	Lewis number (calculated for air)	
L_v	Specific latent heat of vaporisation of water	$\mathrm{J.kg^{-1}}$
m	Mass	kg
$\dot{m}$	Mass flux	$\mathrm{kg.s^{-1}.m^{-2}}$
M_w	Molar mass of water	$\mathrm{kg.mol^{-1}}$
P	Pressure	Pa
$P_{v,sat}$	Saturated water vapour pressure	Pa
$\dot{q}$	Heat flux	$\mathrm{W.m^{-2}}$
R_g	Universal gas constant	$\mathrm{J.mol^{-1}.K^{-1}}$
R	Thermal resistance	$\mathrm{m^2.K.W^{-1}}$
T	Temperature	K
t	Time	s
X_w	Water content (dry basis)	-
ϵ	Product thermal emissivity	-
λ	Thermal conductivity	$\mathrm{W.m^{-1}.K^{-1}}$
ρ	Density	$\mathrm{kg.m^{-3}}$
σ	Stefan-Boltzmann constant	$\mathrm{W.m^{-2}.K^{-4}}$
Subscripts		
mo	Potato moist region	
cr	Potato crust	
dm	Dry matter	
w	Water	
vap	Vapour	
hs	Heating surface	
air	Air	
ref	Reference state	
ct	Contact	
conv	Convection	
rad	Radiation	
boil	Boiling	

1. Introduction

Before their consumption, food products may be subjected to a large number of heat treatments, both at an industrial level and in consumers' own kitchens. In most cases, heat is supplied to the product using one or more of the three elementary modes of heat transfer: thermal convection, thermal radiation and contact heat transfer. While many experimental and theoretical studies have been devoted to thermal convection and radiation, studies concerning contact heat transfer remain relatively rare in the field of food processes. This seems paradoxical since this mode of heat transfer is of prime importance in heating operations such as single- or double-faced grilling or pan-frying and induces drastic product quality changes during heating as shown by Sioen et al. (2006), Haak et al. (2007) and Chevarin et al. (2011) for pan-fried meat or fish and Boskou et al. (2007) for pan-fried potatoes. This lack of information is most likely due to the complexity associated with the experimental characterization and the mathematical formulation of this mode of transfer in the case of heating of food products such as detailed in the following paragraphs.

Generally speaking, contact heat transfer occurs when two solids at different temperatures are put into contact. Because of solid surface irregularities (flatness defects, roughness…), the effective contact surface is necessarily lower than the apparent contact surface (Madhusudana, 1996). At microscopic scale, the interface between two solids can hence be envisioned as a series of contact spots interspersed with gaps that can be either filled with liquid or gas. As proposed by Incropera et al. (2007), the influence of the complex geometry of this interface upon heat transfer between the two solids in contact can be described by the use of a thermal contact resistance R_{ct} or its inverse, a contact heat transfer coefficient h_{ct} defined classically according to:

$$R_{ct} = \frac{1}{h_{ct}} = \frac{|T_A - T_B|}{\dot{q}_{ct}} \quad (1)$$

where $T_A - T_B$ is the temperature gap across the contact interface and $\dot{q}_{ct}$ (calculated as a positive value) is the resulting contact heat flux exchanged between the two solids. This equation is recalled here to illustrate the difficulty to obtain direct measurement of h_{ct} since accurate measurements of the temperature of the two solids at the same interface as well as of the heat flux exchanged between them are required for the calculation, this information being very difficult to obtain without disturbing the phenomenon studied. In practice, the quality of the physical contact between the two solids is likely to change during heating due to the physical or chemical modifications of one of the two materials leading hence to a variation of the thermal contact resistance with time. In the case of food products, this phenomenon is amplified the high reactivity of these materials when subjected to heat treatments. Three types of so called "interfering phenomena" can explain the regular or sudden variation of the thermal contact resistance during contact heating of food products: (i) the deformation of the heated surface of the product as for example in the case of meat grilling when the heated muscle retracts (Housova and Topinka, 1985), (ii) the formation of a crust at the lower surface of the product due to a local and drastic drying of the product in this zone, this crust interfering with heat and mass transfer phenomena at this location (Feyissa et al., 2011) and (iii) the release of liquid water or water vapour at the interface between the heated product and the heating surface as experimentally observed by Cernela et al. (2015).

To obtain direct measurement of instantaneous values of thermal contact resistance in the case of food products, several methods have been found in the literature. The most commonly used is based on the positioning of (i) a surface heat flux sensor between the food product and the

heating surface and (ii) one thermocouple in the product and one in the heating surface, these two thermocouples being as close as possible to the contact interface (Housova and Topinka, 1985; Wichchukit et al., 2001; Pan and Singh, 2002). These measurements make it possible to calculate instantaneous values of thermal contact resistance using Eq. 1. However, significant drawbacks of this method can be identified: (i) the local disturbance of the transfer phenomena induced by the presence of the sensor between the two solids making the flux measurement invasive, (ii) the difficulty to measure precisely the temperature of the heated product at a distance of its lower surface which can be considered small enough in regard to the very high temperature gradient in this zone.

Another option consists in associating experimental measurements with a mathematical model describing heat and mass transfer phenomena within the product, thereby allowing to calculate the temperature of its lower surface. The estimation of the thermal contact resistance is thus performed by comparing experimental and calculated results. To be successful, this method requires an accurate description of the transfer phenomena occurring in the product and especially in the zone close to the heating surface. Some authors, such as Zorrilla & Singh (2000), Banga et al. (2001), Zorrilla & Singh (2003), Huang (2012) and Eberth et al. (2012), have used this method to evaluate the thermal contact resistance. However, the main limitation of these studies is that the models proposed do not consider the coupling between heat transfer and the (possibly intense) evaporation of water exuding from the product at its lower surface. Only three authors have proposed models that take this phenomenon into account (Ou and Mittal, 2006; Dhall and Datta, 2011; Feyissa et al, 2011). It was taken into account: (i) by using an expression similar to the one encountered in convective drying even though the existence of a boundary layer relative to mass transfer is questionable in the interfacial zone (Ou and Mittal, 2006 and Dhall and Datta, 2011) or (ii) by considering the rate of liquid water removed from

the product and the rate of water vapour generated at the contact interface both equal to the rate of evaporation (Feyissa et al., 2011). In these studies, water evaporation is also considered in the whole product. To describe it, Ou and Mittal (2006) and Feyissa et al. (2011) assumed that liquid water was in equilibrium with water vapour in the product whereas Dhall and Datta (2011) opted for a non-equilibrium formulation.

Based on the above limitations concerning both experimental strategies and modelling approaches, one of the objectives of the present work is to clarify the coupled heat and mass transfer phenomena occurring during contact heating (and by extension pan frying) of potato slices. To reach this aim, contact heating experiments were conducted and a particular attention was paid to obtaining reliable and repeatable measurements of the product temperatures and water loss during heating. The choice of potato as tested material was made because, despite the fact that this product is very often heated by contact, this mode of heat transfer applied to this product has been very rarely studied in the literature. To gather rich and varied experimental data, two operating factors expected to influence contact heat transfer have been studied: the heating power supplied to the potato disk and the presence or not of an oil layer below this product.

Another objective of the work is to identify, among all the transport phenomena of concern, the one limiting the overall heating of the product allowing to determine rational strategies in order to improve the sensory and nutritional qualities of the products heated by contact.

Finally, the last objective of the work is to determine, using a non-invasive method, the values of the contact heat transfer coefficient between the product and the heating surface. To reach this aim, an approach combining experimental characterization and modelling is proposed. The model developed in this study considers the formation and propagation within the product of a water boiling front and the resulting development of a dried crust in the lower zone of the

product, a special care having been taken to limit as much as possible the number of unknown parameters of the model.

2. Materials and methods

2.1. Laboratory contact heating device

For the purpose of this study, a heating device was designed based on the experimental set-up proposed by Ashokkumar and Adler-Nissen (2011) and also used by Feyissa et al. (2011) and Sanz-Serrano et al. (2017) to perform contact heating experiments under controlled conditions. However, a slight modification was made to this experimental set-up by positioning a 1 mm K-type thermocouple as close as possible to the heating surface in order to obtain direct measurement of its temperature. A schematic representation of the device is presented in Fig. 1. It consists of a four-disc assembly placed inside a calcium silicate insulating jacket. The assembly is obtained by using bolts and nuts not shown on Fig. 1. From bottom to top, this assembly comprises a polyether ether ketone (PEEK) disc, a calcium silicate insulating sheet, a surface heating resistance (HM 4974 MICA Heater, Minco, Aston, United-States) and an aluminium disc (so called “heating surface” in the following text) on which the potato sample is put during the experiment. This aluminium disc is surrounded by a Teflon rim to contain the potential flows of oil or cooking juices during heating. The surface heating resistance can supply a homogeneous heating power that can reach up to 170 $kW.m^{-2}$. This power can be either fixed at a constant value or adjusted using a PID controller in order to regulate the temperature of the upper aluminium disc. In the latter case, the PID controller uses the temperature measured by the 1 mm K-type thermocouple positioned at the centre of the heating surface as measured process variable.

156

157 *2.2. Preparation of the potato sample*

158

159 For the experiments, Caesar potatoes were purchased at a local supermarket (Cora, Massy,
160 France) and stored at room temperature (20°C ± 2°C) for no longer than ten days. Before
161 heating, potatoes were cut into thick cylindrical slices using a cylindrical cutting shape and then
162 into thin slices using an electric slicer. Each sample had a diameter of 45 mm and a height of
163 15 mm.

164

165 *2.3. Protocol for the contact heating experiment*

166

167 Before each experiment, the aluminium disc of the heating device was pre-heated to a constant
168 temperature of 180°C using the PID controller described in § 2.1. For each heating test, a
169 waiting time of 15 minutes before the start of the experiment was then observed to ensure the
170 repeatability of the initial conditions of the test. At the end of the pre-heating phase, for
171 experiments with oil, 1 g of sunflower oil was put in the centre of the heating surface. The
172 potato sample was then placed at the centre of the heating surface and the heating power was
173 immediately set to a constant value (either 3.2 $kW.m^{-2}$, 6.4 $kW.m^{-2}$ or 9.6 $kW.m^{-2}$) until the end
174 of the experiment. These values were chosen in order to reproduce the patterns of variations of
175 heating surface temperature experimentally recorded during home-scale pan-frying operations
176 (Cernela et al., 2014). The heating time was fixed to 15 min for the lower and intermediate
177 power value (3.2 $kW.m^{-2}$, 6.4 $kW.m^{-2}$) and limited to only 10 min for the upper power value
178 (9.6 $kW.m^{-2}$) in order to avoid overheating of the experimental setup.
179 In summary, six operating conditions were thus tested by combining the three tested heating
180 powers with or without addition of vegetal oil below the product at the beginning of heating.

Each condition was repeated 10 times in order to evaluate standard deviations values for measured values.

2.4. Mass and temperature measurements during experiments

To measure the mass variations of the potato sample during heating, the whole heating device was put on a SG8001 precision balance (Mettler Toledo, Viroflay, France) with a measurement sensibility of 0.1 g. The mass variations obtained by the balance was considered equal to the water loss by the potato sample during the test.

The temperature of the potato samples was evaluated at three locations using 0.25 mm diameter K-type thermocouples. These 3 measurement points were all located on the central axis of symmetry of the cylinder at a distance of 3 mm, 6.5 mm and 11 mm from the bottom surface of the product. In order to obtain precise position of the thermocouples, pre-holes were made horizontally within the potato cylinder using a 0.8 mm diameter metal rod. The thermocouples were then inserted until the end of these pre-holes. The uncertainty associated with the position of the thermocouples was evaluated at $\pm$ 0.5 mm by precisely measuring 10 times their positions after having cut the potato cylinder in two in the thickness direction.

As already mentioned, the temperature of the aluminium disk was measured using a K-type thermocouple. Given the high thermal conductivity of aluminium (200 $W.m^{-1}.K^{-1}$), the thermocouple was positioned close enough to the upper surface of the aluminium disc to consider that its temperature is equal to the heating surface temperature.

All data were obtained using a sampling time equal to one second.

3. Mathematical model

3.1. Modelling approach and global assumptions

The following modelling approach is used to describe complex coupled heat and mass transport phenomena occurring during contact heating. At the beginning of the heating test, the lower surface of the potato sample is put into contact with a surface at high temperature and is hence subjected to a very strong heat flux. Due to the relatively low values of the thermal conductivity of food products (0.6 $W.m^{-1}.K^{-1}$ for potato as measured by Gratzek & Toledo, 1993), the temperature of the lower surface is expected to increase rapidly. When the temperature of the lower surface reaches the boiling temperature of water at atmospheric pressure (100°C), a boiling front is formed on this surface and propagates toward the interior of the product during the remaining time of the heating, as explained by Farkas (1994) or Farid (2002). In the model, the boiling front is described by the use of a sharp interface, moving in the product, where all the internal evaporation happens. It divides the product into two regions: an initially moist region above the sharp interface and a dried region (so called crust) below it. The crust is also defined by two criteria (i) a concentration of liquid water that can be assumed negligible and (ii) a temperature which can be higher than the boiling temperature of water. To justify the first criterion, it is important to note that the possible presence of bound water in the crust after boiling is not important for this study since this bound water fraction is also not taken into account when measuring the initial water content of the sample.

Finally, as shown in Fig. 2, the heating process is broken down into two stages: (1) a stage during which the lower surface of the product is heated up to 100°C and (2) a stage where a boiling front is formed and propagates through the product during heating.

To agree with the observations made during the experiments and to simplify the mathematical formulation of the transfer phenomena, further assumptions were made:

(1) Given the geometry of the potato sample, heat and mass flux are expressed in 2D cylindrical system of coordinates

(2) In the moist region, the product is constituted by dry matter, liquid water and negligible amount of gas whereas in the crust region, the product is only constituted by dry matter, negligible amount of liquid water and water vapour (produced at the boiling front)

(3) Given the low thickness and the significant porosity of the crust, the resistance to water vapour transfer in this zone is assumed negligible. The liquid water evaporated at the position of the boiling front is thus assumed to be instantly evacuated from the product.

(4) Heat transfer in the crust is considered to occur in quasi-steady-state regime since the energy consumed by the crust to raise its temperature (sensible energy), is usually very small compared to the energy consumed by water evaporation at the position of the boiling front (Farid, 2002). According to this assumption, the temperature profile within the crust is assumed linear. The heat flux through it is calculated using a global thermal resistance adding the resistance induced by thermal conduction within the crust and the thermal contact resistance

(5) Temperature at the boiling front is assumed equal to 100°C which also means that the sudden vaporization of water by boiling mechanism occurs at atmospheric pressure within the product

(6) Noticing by simple visual observation that the product does not suffer major volume changes during heating, shrinkages of the porous solid network constituting the crust and of the rest of the moist product are assumed negligible

3.2. Stage 1: initial heating

3.2.1. Governing equations

During initial heating, heat and water transfers in the moist region of the product are described using the following conservation equations (Eq. 2).

$$\begin{cases} \rho_{dm} \dfrac{\partial X_w}{\partial t} + \vec{\nabla}.\overrightarrow{\dot{m}_w} = 0 \\ \rho_{dm} \dfrac{\partial \widehat{H}}{\partial t} + \vec{\nabla}.\vec{\dot{H}} = 0 \end{cases} \quad (2)$$

As water is considered to move only under the effect of concentration gradients, the mass flux of water is written according to Fick's law:

$$\overrightarrow{\dot{m}_w} = -\rho_{dm} D_w \vec{\nabla} X_w \quad (3)$$

Concerning heat transfer, $\widehat{H}$ refers to the total enthalpy by unit-mass of dry matter and is calculated according to:

$$\widehat{H} = Cp_{dm}(T - T_{ref}) + X_w Cp_w(T - T_{ref}) \quad (4)$$

The enthalpy flux density appearing in Eq. 2 is the sum of the conduction flux (calculated according to Fourier's law) and of the enthalpy flux associated with the flux of liquid water inside the product:

$$\vec{\dot{H}} = -\lambda_{mo} \vec{\nabla} T + Cp_w(T - T_{ref})\, \overrightarrow{\dot{m}_w} \quad (5)$$

3.2.2. Boundary condition at the upper and lateral surface

At the upper ($z = z_{max}$) and lateral surfaces ($r = R_{max}$) of the product, the product is in contact with ambient air and some convective drying occurs described using:

$$\overrightarrow{\dot{m}_w}.\vec{n} = k\frac{M_w}{R_g}\left(\frac{a_w(X_w,T)P_{vsat}(T)}{T} - \frac{p_{v,air}}{T_{air}}\right) \text{ at } z = z_{max} \text{ or at } r = R_{max} \quad (6)$$

where $\vec{n}$ is the unit vector normal to the surface of concern. For these boundaries, the enthalpy flux in the product is expressed as the sum of the convective and radiative flux exchanged with the surrounding minus the energy consumed by the evaporation of liquid water reaching the surface of the product:

$$-\lambda_{mo}\vec{\nabla}T.\vec{n} = h(T - T_{air}) + \varepsilon\sigma\left(T^4 - T_{rad}^4\right) + L_v(T)\,\dot{m}_w \text{ at } z = z_{max} \text{ or at } r = R_{max} \quad (7)$$

where $L_v(T)$ is the specific latent heat of vaporisation of water and *h* is the convective heat transfer coefficient. The values of *h* were calculated using the Nusselt correlations for free convection in flat and cylindrical geometries at the upper and lateral surfaces respectively (Incropera et al., 2007). The relations used to calculate these coefficients are given in the appendix section. The obtained values are very low at the beginning of heating because of the small difference between the product temperature and the air temperature and increase up to around 10 $W.m^{-2}.K^{-1}$ at the end of heating when the upper and lateral surfaces reach an average value of around 40°C.

3.2.3. Boundary condition at the lower surface

During this short stage and due to the roughness of the product lower surface, the convective drying of this surface within the small gas gaps located between it and the heating surface is

assumed to have a negligible effect on product overall moisture loss. At the same interface, the heat flux transferred to the product by the heating surface is given by the following equation.

$$-\lambda_{mo}\vec{\nabla}T.\vec{n} = h_{ct}(T_{hs}(t) - T) \text{ at } z = 0 \quad (8)$$

where T_{hs} is the temperature of the heating surface obtained by a linear interpolation of the discrete measurement of the aluminium disk temperature.

3.3. Stage 2: Moving of a boiling front through the product

Governing equations in the moist region and boundary conditions at the upper and lateral surface are identical for both stages. The heat transfer being assumed to occur in steady state regime in the crust and the water vapour having been assumed to be transported in the crust with no resistance (as discussed in § 3.1), no boundary condition is required for the crust layer formed below the product. Considering the definition of the boiling front, the boundary condition for heat transfer at this location is:

$$T = T_{boil} = 100°C \; at \; z = e_{cr}(t) \quad (9)$$

The water diffusion from the moist region to the boiling front is neglected in comparison with the local evaporation rate due to boiling. The liquid water of the crust being assumed equal to zero, the advance of the boiling front is hence used to calculate the instantaneous water loss at this location. This is expressed according to:

$$\dot{m}_{vap} = \rho_{dm} X_w \frac{\partial e_{cr}}{\partial t} \quad (10)$$

The boundary condition for the heat balance is used to calculate the local velocity of the boiling front within the product. This local velocity is assumed to be only on the z-axis but depends on the radial position. It is calculated according to:

$$\rho_{dm} X_w \frac{\partial e_{cr}}{\partial t} L_v = \left(\overrightarrow{\dot{q}_{cr}} - \lambda_{mo} \vec{\nabla} T\right).\vec{n} \quad (11)$$

where $-\lambda_{mo}\vec{\nabla}T$ is the conductive heat flux in the moist region at this location and $\overrightarrow{\dot{q}_{cr}}$ is the conductive heat flux through the crust. This heat flux is calculated by using an equivalent thermal resistance $R_{th,eq}$ globalising the thermal contact resistance $R_{th,ct}$ between the product and the heating surface and the crust thermal resistance $R_{th,cr}$ as written in Eqs. 14 and 15.

$$\overrightarrow{\dot{q}_{cr}}.\vec{n} = \frac{1}{R_{th,eq}}(T_{hs}(t) - T_{boil}) \quad (12)$$

$$\text{with } R_{th,eq} = R_{th,ct} + R_{th,cr} \quad (13)$$

$$R_{th,ct} = \frac{1}{h_{ct}} \text{ and } R_{th,cr} = \frac{e_{cr}}{\lambda_{cr}} \quad (14) \text{ and } (15)$$

3.4. Model solving

The model equations were solved using COMSOL Multiphysics v 5.3 software COMSOL AN, Stockholm, Sweden) in a 2D-axisymetric geometry for the domain occupied by the moist region of the product. The mesh was deformed following the moving boundary (boiling front). The mesh size sensitivity was investigated by solving the model after having meshed the domain with 4268 and 16 946 free triangular elements. A difference of less than 0.2°C was obtained

for the temperatures calculated after 15 min of heating at the positions of the thermocouples placed in the potato sample.

The values of parameters and the mathematical relations used in the model are listed in the appendix section. This information was either gathered from the literature or obtained from experimental measurements. Only the contact heat transfer coefficient was considered as an unknown parameter. Its value was assumed different for contact heating with and without oil in order to take into account the anticipated impact of the oil layer on contact heat transfer between the product and the heating plate. These two values were estimated following the calibration procedure described in the next section.

3.5. Calibration and validation procedure

The model was calibrated and validated using the product temperatures and the water loss measurements.

The two values of the contact heat transfer coefficient were estimated from the experiments performed at a heating power of 3.2 $kW.m^{-2}$ with and without oil respectively and so achieve the model calibration. The estimation was performed using the least square method which consists of finding the parameter value that minimizes the quadratic error between simulated and experimental results. The Levenberg-Marquadt non-linear regression algorithm (within the Matlab© environment), suited for non-linear estimation problems, was used to achieve the minimization and calculate the non-linear confidence intervals.

The model was validated using the experimental data obtained at the other heating powers (6.4 $kW.m^{-2}$ and 9.6 $kW.m^{-2}$) to evaluate its ability to predict results in different operating conditions. The validation was performed by comparing graphically the experimental and simulation results. An index of the fitness quality was calculated for each operating condition

in order to support the graphical comparison. The chosen index is the mean absolute error (MAE) of the model because it gives a good representation of the difference observed between experimental and simulation results. This was calculated separately for water loss and food product temperatures according to Eq. 16.

$$MAE = \frac{1}{N-1}\sum_{1}^{N}\left|\widehat{Y}_i - Y_i\right| \quad (16)$$

Where Y_i is the experimental value, $\widehat{Y}_i$ is the prediction value and N is the number of data.

4. Results and discussion

4.1. Experimental results

The objective of this section is to evaluate the impact of the heating power and of the presence or not of the oil layer on heat and mass transfer in the product during heating. The experimental results are presented in Fig. 3 where mean values and standard deviations are plotted with a sampling interval of 15 s and 120 s respectively.

The heating surface temperature variations obtained for all the operating conditions are presented in Fig. 3a. The heating power has a major influence on the kinetic of the heating surface temperature. At the beginning of the experiment, the heat transferred to the product is higher than the one supplied by the heating resistance leading to an initial decrease of the heating surface temperature for any heating power tested. For the lowest heating power, this temperature reaches a nearly constant value of *circa* 145°C after 5 min. For the two higher heating powers of 6.4 kW.m^{-2} and 9.6 kW.m^{-2}, the temperature of the heating surface rises

continuously after its initial decrease to reach a value of about 200°C and 245°C after 10 min of heating.

The presence or not of an oil layer below the product has a significant impact on the initial temperature drop. This drop is about 8°C without oil and about 13°C with oil for a heating power of 6.4 $kW.m^{-2}$. Later in the heating, the presence of an oil layer is less influential than the modification of the heating power. Since the oil layer is expected to enhance heat transfer to the product, the heating surface temperature is constantly lower for experiments with oil than for the ones without oil. At 600 s, the difference goes from about 5°C at 3.2 $kW.m^{-2}$ to 10°C at 9.6 $kW.m^{-2}$.

Fig. 3b shows the water losses measured for all the operating conditions. These are significantly higher for experiments at 6.4 $kW.m^{-2}$ than for those at 3.2 $kW.m^{-2}$. At 600 s, the difference is about 0.8 g for experiments with oil and about 0.5 g for experiments without oil. This result is in line with our expectations since the increase in water losses obtained when increasing the heating power has already been reported in several studies concerning contact heating of food product (Feyissa et al., 2011; Cernela et al, 2015; Rocca et al., 2019). In contrast, water losses measured at the highest heating power (9.6 $kW.m^{-2}$) do not behave as expected. At 600 s, the water loss is almost the same with and without oil and lower than the one with oil at 6.4 $kW.m^{-2}$. At this level of heating power, water evaporation seems to be limited by the formation of an over-heated and over-dried material crust at the lower surface of the product opposing, for this operating condition only, an efficient resistance to overall mass transfer. This phenomenon will be more quantitatively discussed from the analysis of the results calculated by the model.

The influence of the presence of oil on water loss is significant for the two smallest heating powers. At 600 s, the difference between experiments with and without oil is about 0.3 g at 3.2 $kW.m^{-2}$ and 0.6 g at 6.4 $kW.m^{-2}$. This agrees with the observation made on heating surface

411 temperature. As expected, the presence of the oil layer increases the level of heat transferred to
412 the product, which implies a higher evaporation rate of the water in the product.
413
414 The measurements obtained from the three thermocouples located at 3, 6.5 mm and 11 mm
415 from the product's lower surface are plotted in Fig. 3c for experiments with oil and in Fig. 3d
416 for experiments without oil. The heating power seems to have little influence on the temperature
417 measured in the product even for the lower thermocouple. At the end of heating, the largest
418 difference observed for the three heating powers tested is only *circa* 5°C for all considered
419 locations. The sensible heat (related to product temperature changes) accumulated by the
420 product is thus relatively the same independently the power supplied. This result has also been
421 reported by Feyissa et al. (2011) for temperatures measured away from the contact interface
422 only. When the thermocouple is located close enough to the contact interface, the effect of the
423 heating power is very marked as soon as the temperature exceeds the boiling point of water
424 (around 100 ° C in the product). Elsewhere, the temperatures increase similarly to those shown
425 here since they tend asymptotically towards 100°C. This suggests hence that a large part of the
426 heat received by the product is not used to raise its sensible energy but consumed by the
427 evaporation of the water contained in it as mentioned by Feyissa et al. (2011). This is also in
428 line with the hypothesis of a boiling front at 100°C moving from the lower surface to the inner
429 parts of the product.
430 The temperatures measured in the product are also affected to a small extent by the presence or
431 not of an oil layer. The largest observed difference between the curves is about 4°C whatever
432 the location of measurement considered. As for the heating power, the additional heat received
433 when heating the product with oil seems largely consumed by the vaporisation of water within
434 the product.
435

436 *4.2. Estimation of the contact heat transfer coefficient*

437

438 Following the calibration procedure described in § 3.5, the food product temperatures and the
439 water loss measured at 3.2 $kW.m^{-2}$ were used to estimate both values of the contact heat transfer
440 coefficient. The results of the estimation, presented as nominal value $\pm$ confidence interval of
441 the parameter, are: 197.5 ± 5.8 $W.m^{-2}.K^{-1}$ for contact heating without oil and 512.2 ± 12.4
442 $W.m^{-2}.K^{-1}$ for contact heating with oil. As a remark, the confidence interval obtained for contact
443 heating with oil is higher than the one without oil. This greater uncertainty can be explained by
444 the higher value of the Biot number (6.4 with oil compared to 2.5 without oil at the beginning
445 of heating) which indicates that, in this case, the contact heat transfer coefficient has less
446 influence on heat transfer in the product and therefore on the simulation results.
447 From a literature perspective, the estimated values are in the range of contact heat transfer
448 coefficients found in the field of contact heating of food products (from ~ 100 $W.m^{-2}.K^{-1}$ to
449 more than 1000 $W.m^{-2}.K^{-1}$). The value obtained for contact heating without oil is similar to
450 those measured by Housova and Topinka (198), Wichchukit et al. (2001) and Pan and Singh
451 (2002) for meat grilling at the early stage of the process. During this stage, water and fat are
452 still in the product and the gaps between the product and the heating surface are filled with air.
453 During heating, the meat product releases water and fat. The contact heat transfer coefficient
454 measured by these authors thus increase sharply to reach values comparable to the one
455 estimated for contact heating with oil. The results obtained are in line with the observations
456 made by these authors. These make it possible to quantify in term of order of magnitude the
457 impact of a fat layer on contact heat transfer between a food product and a heating plate.

458

459

460

461 *4.3. Model validation*

462

463 The model was solved for each operating condition using the above estimated values of the
464 contact heat transfer coefficient. As explained in § 3.5, experimental measurements and
465 simulated values of food product temperatures and water loss were plotted in order to evaluate
466 the quality of the model predictions (Figs. 4-6). Index of fitness quality were also calculated to
467 support the graphical comparisons.

468

469 For the operating conditions used to calibrate the model (3.2 $kW.m^{-2}$ with and without oil),
470 calculated and measured values are shown in Fig. 4. The model predictions are in good
471 agreement with the experimental measurements. The mean absolute errors calculated for water
472 loss are 0.1 g with oil and 0.2 g without oil while the mean absolute errors for food product
473 temperatures are 3.3°C with oil and 2.4°C without oil. Only the temperature calculated at the
474 upper position in the product slightly deviates from the measured data. Because of its location,
475 this temperature measurement is significantly influenced by convection heat transfer occurring
476 between the upper and lateral surfaces of the product and the surrounding air. The deviation
477 observed is thus partly the consequence of the approximations made when calculating the heat
478 and mass transfer coefficients for these surfaces. An experimental characterisation of these
479 coefficients in the conditions of the present experiments could probably help to decrease this
480 deviation.

481

482 Results for the operating conditions at 6.4 $kW.m^{-2}$ and 9.6 $kW.m^{-2}$ (with and without oil) are
483 shown in Fig. 5 and Fig. 6 respectively. Although the model was not calibrated using these
484 operating conditions, the model predictions are also satisfactory. The mean absolute errors for
485 the food product temperatures are in the same order of magnitude as for the operating conditions

at 3.2 $kW.m^{-2}$. They are equal to 3.3°C with oil and 2.5°C without oil at 6.4 $kW.m^{-2}$ and are equal to 3.7°C with oil and 2.3°C without oil at 9.6 $kW.m^{-2}$. In contrast, the mean absolute errors for water loss are higher as the heating power increases. At 6.4 $kW.m^{-2}$, the values are 0.2 g with oil and without oil. At 9.6 $kW.m^{-2}$, they are 0.4 g with oil and without oil. The model loses in prediction quality mainly at 9.6 $kW.m^{-2}$ (Fig. 6b) where the water loss is sensibly overestimated by the model, especially when the experimental values of product water loss levels off between 50 s and 200 s. At this power level, the drastic temperature rise at the lower surface of the product seems to have resulted in the formation of an over-heated crust limiting significantly the evacuation of water produced within the product at this location. This point having not yet been included in the model, the introduction of a mass transfer resistance corresponding to the role played by the crust in overall mass transfer could increase the accuracy of the present model. However, at this point of investigation and given the limits of the experimental data available, considering this phenomenon remains a tricky problem.

4.4. Use of the model for a better understanding of limiting phenomena during contact heating

Model validation shows the relevance of using a moving front approach to describe heat and mass transfer in the product during contact heating. The main interest of this approach is to take into account the boiling phenomenon occurring in the zone of the product close to the heating surface with few computational effort and a reduced number of parameters to be estimated compared to the distributed evaporation approach used by Dhall and Datta (2011) for example. To illustrate the simulation results obtained, Fig. 7 shows the temperature and the water content distribution calculated by the model at 900 s for the operating condition at 3.2 $kW.m^{-2}$ with oil. From the observation of these results, two main features and characteristics of contact heating applied to potato can be deduced.

Firstly, a large part of the heating power supplied to the product is consumed by water evaporation within the product (at the location of the boiling front in the model developed here). As proof of that, Tab. 1 compares, for each operating condition, the amount of energy transferred to the product and converted into sensible heat E_{sens} or consumed by the evaporation of water E_{vapo}. Both energies were evaluated by calculations made after 600 s of heating. Except for the heating power of 3.2 kW.m^{-2} without oil, E_{sens} is always lower than E_{vapo}. For the high heating power (9.6 kW.m^{-2}), E_{sens} is half of E_{vapo}. These results are in lines with the observations made by Feyissa et al. (2011) for pancake frying and Rocca et al. (2019) for meat grilling. In both studies, at the end of the heating process, the heat consumed by evaporation of the water inside the product is also much higher than the heat used to rise its sensible energy. The result obtained on the potato, added to the ones already published on other products, suggest that this aspect is characteristic of the contact heating process.

It can also be noted that E_{sens} is very slightly influenced by the operating conditions unlike E_{vapo}. This agrees with the fact that both the presence of an oil layer and the variations of the heating power have a little impact on temperature rise kinetics in the moist region of the product and a much greater impact on the amount of water evaporated during heating.

Secondly, the boiling front is also responsible for the development of a dry and thermally-insulating crust. At 600 s, the crust thickness calculated by the model is 0.50 mm, 1.1 mm, 1.5 mm for experiments without oil at 3.2 kW.m^{-2}, 6.4 kW.m^{-2} and 9.6 kW.m^{-2} respectively and 0.72 mm, 1.3 mm, 1.7 mm for experiments with oil at 3.2 kW.m^{-2}, 6.4 kW.m^{-2} and 9.6 kW.m^{-2} respectively. Because of its low thermal conductivity (0.1 W.m^{-1}.K^{-1}), the formed crust acts as a thermal resistance ($R_{th,cr}$ in Eq. 15) between the heating surface and the moist region of the product. This thermal resistance is added to the thermal contact resistance ($R_{th,ct}$ in Eq. 14)

after the formation of the crust. The values of these two thermal resistances during heating have been plotted in order to evaluate their influence on overall heat transfer to the product for each operating condition. Results are shown in Fig. 8. Since the thermal resistance of the crust depends on its thickness, $R_{th,cr}$ increases during heating. For all operating conditions, two phases of heating can then be considered. A first phase where the contact heat transfer resistance $R_{th,ct}$ is predominant and a second phase when it is quite substantially exceeded by the crust thermal resistance $R_{th,cr}$.

With oil, $R_{th,cr}$ exceeds $R_{th,ct}$ after only 30 seconds of heating. After 600 s of heating, this resistance is from 4 or 9 times higher than $R_{th,ct}$. In these conditions, the influence of the contact heat transfer is nearly negligible compared with the one induced by the crust. In these conditions only, the model could potentially be simplified by assuming that $R_{th,ct}$ is zero which is equivalent to consider that the physical contact is ideal between the heating surface and the product.

Without oil, the $R_{th,cr}$ becomes higher than $R_{th,ct}$ after heating times ranging from 200 s to 600 s and the difference between the two values is less significant than for the experiments with oil at the end of heating (from 1.5 to 3 times higher). In these conditions, the contact heat transfer still has a significant influence on the overall heat transfer to the product. Both contact heat transfer and heat conduction into the crust need then to be considered in the model to obtain correct predictions of temperature rise and water loss.

5. Conclusion

A 2D mathematical model using a moving boiling-front approach was developed in this study to describe heat and mass transfer during contact heating of potato slices. This model is relatively simple to implement and requires only one parameter to be estimated (the contact

heat transfer coefficient). It was validated by showing satisfying agreements between simulation results and experimental data, in view of the simplifying assumptions of the model. The simulations results highlight the expected strong impact of the presence of the oil layer between the product and the heating surface. They also attest the fact that the overall heating of the product is mainly limited: (i) by the evaporation of liquid water at the location of the boiling front and (ii) by the development of a dried zone in the lower part of the heated product acting as a thermal insulating layer.

However, there are still some doubts concerning the assumption of a negligible resistance to water vapour transfer in the crust formed under the product during heating. At high heating power, the crust seems indeed to limit water transfer at the beginning of the treatment more than at lower heating powers, which leads to an overestimation of water losses under these conditions. This still limits the predictive abilities of the model and would be the subject of further studies. In particular, visible optical microscopy is planned to characterise the porous structure of the crust and better understand its influence on vapour transfer properties such as permeability.

Acknowledgements

This work was funded by the French National Research and Technology Agency (ANRT).

580 **Appendix: values of parameters and mathematical relations used in the model**

Parameter	Definition	Value	Source
Cp_{wG}	Specific heat of water vapour	$2.03\ \mathrm{kJ.kg^{-1}.K^{-1}}$	
Cp_{wL}	Specific heat of liquid water	$4.18\ \mathrm{kJ.kg^{-1}.K^{-1}}$	
Cp_{dm}	Specific heat of dry matter	$1.8\ \mathrm{kJ.kg^{-1}.K^{-1}}$	Wang & Brennan (1993)
D_w	Effective water diffusivity	$1.10^{-9}\mathrm{m^2.s^{-1}}$	Ronald et al. (1992)
$L_v(T_{ref})$	Latent heat of vaporization at reference temperature	$2.454.10^6\ \mathrm{J.kg^{-1}}$	
M_w	Molar mass of water	$1.8.10^{-2}\ \mathrm{kg.mol^{-1}}$	
$P_{w,air}$	Partial pressure of water in air	1170 Pa	
R_g	Gas constant	$8.314\ \mathrm{J.mol^{-1}.K^{-1}}$	
T_0	Product initial temperature	20°C, assumed uniform	Measured
$T_{air,lateral}$	Air temperature at the lateral surface of the product	50°C	Measured at 10 mm from the lateral surface
$T_{air,upper}$	Air temperature at the upper surface of the product	30°C	Measured at 10 mm from the upper surface
T_{rad}	Equivalent temperature of radiation	20°C	Room temperature (measured)
T_{ref}	Reference temperature	20°C	Room temperature (measured)
X_0	Product initial moisture content (dry basis)	3.65, assumed uniform	Golmohammadi and Afkari-Sayyah (2013) for Caesar potatoes
ε	Product emissivity	0.9	Assumed
λ_{mo}	Thermal conductivity of the moist region	$0.6\ \mathrm{W.m^{-1}.K^{-1}}$	Gratzek & Toledo (1993)
λ_{cr}	Thermal conductivity of the crust	$0.1\ \mathrm{W.m^{-1}.K^{-1}}$	Califano & Calvelo (1993)
ρ_{dm}	Density of dry matter in the product	$223\ \mathrm{kg.m^{-3}_{prod}}$	Golmohammadi & Afkari-Sayyah (2013)
ρ_w	Density of water in the product	$837\ \mathrm{kg.m^{-3}_{prod}}$	Golmohammadi & Afkari-Sayyah (2013)
σ	Stephan-Boltzmann constant	$5.67.10^{-8}\ \mathrm{W.m^{-2}.K^{-4}}$	

581

Relation	Definition	Equation	Source
a_w	Water activity	$a_w = 1 - e^{-0.075TX_w^{1.44}}$	
h_{upper}	Convective heat transfer coefficient at the upper surface of the product	$h_{upper} = 4.19.\left\|T - T_{air,upper}\right\|^{0.25}$	Empirical correlation (Incorpera et al., 2007)
$h_{lateral}$	Convective heat transfer coefficient at the lateral surface of the product	$h_{lateral} = 2.96.\left\|T - T_{air,lateral}\right\|^{0.25}$	Empirical correlation (Incorpera et al., 2007)
k_{upper}	External mass transfer coefficient at the upper surface of the product	$k_{upper} = \frac{h_{upper}}{\rho_{air} Cp_{air} Le^{2/3}}$	Chilton-Colburn analogy
$k_{lateral}$	External mass transfer coefficient at the lateral surface of the product	$k_{lateral} = \frac{h_{lateral}}{\rho_{air} Cp_{air} Le^{2/3}}$	Chilton-Colburn analogy
L_v	Specific Latent heat of vaporization	$L_v = L_v(T_{ref}) + (Cp_{wG} - Cp_{wL})(T - T_{ref})$	
$P_{v,sat}$	Saturated vapour pressure	$P_{v,sat} = 101325\ (17.443 - \frac{2795}{T} - 3.868.Log_{10}(T))$	Dupré-Bertrand law

582

583 **References**

584 Ashokkumar, S., & Adler-Nissen, J. (2011). Evaluating non-stick properties of different surface
585 materials for contact frying. *Journal of Food Engineering*, *105*(3), 537-544.

586 Banga, J. R., Pan, Z., & Singh, R. P. (2001). On the Optimal Control of Contact-Cooking
587 Processes. *Food and Bioproducts Processing*, *79*(3), 145–151.

588 Boskou, G., Salta, F. N., Chiou, A., Troullidou, E., & Andrikopoulos, N. K. (2006). Content of
589 trans,trans-2,4-decadienal in deep-fried and pan-fried potatoes. *European Journal of Lipid*
590 *Science and Technology*, *108*(2), 109–115.

591 Califano, A. N., & Calvelo, A. (1993). Thermal Conductivity of Potato between 50 and 100°C.
592 *Journal of Food Science, 56*(2), 586-587.

593 Cernela, J., Heyd, B., & Broyart, B. (2014). Evaluation of heating performances and associated
594 variability of domestic cooking appliances (oven-baking and pan-frying). *Applied*
595 *Thermal Engineering*, *62*(2), 758–765.

596 Cernela, J., Heyd, B., Keller, S., Bailleul, J. L., Maillard, M. N., Bonazzi, C., & Broyart, B.
597 (2015). Experimental study of heat and mass transfer phenomena during the contact
598 heating of solid food models. *Journal of Food Engineering*, *146*, 99–106.

599 Chevarin, C., Bonny, J. M., Kondjoyan, A., Thomas, A., Bauchart, D., Portanguen, S., &
600 Clerjon, S. (2011). Oil uptake by beef during pan frying: Impact on fatty acid composition.
601 *Meat Science, 91*(1), 79–87.

602 Dhall, A., & Datta, A. K. (2011). Transport in deformable food materials: A poromechanics
603 approach. *Chemical Engineering Science*, *66*(24), 6482–6497.

Eberth, J. F., Neal, J. A., & Robles Hernandez, F. C. (2012). Evaluation of heat propagation through poultry in a reduced computational-cost model of contact cooking. *International Journal of Food Science and Technology*, *47*(6), 1130–1137.

Farid, M. (2002). The moving boundary problems from melting and freezing to drying and frying of food. *Chemical Engineering and Processing: Process Intensification*, *41*(1), 1–10.

Farkas, B. E. (1994). Modeling immersion frying as a moving boundary problem. Ph.D. Dissertation, University of California, Davis.

Farkas, B.E., Singh, R.P. and Rumsey, T.R., (1996). Modeling heat and mass transfer in immersion frying, I. Model development. *Journal of Food Engineering*, *29*, 211–226.

Feyissa, A. H., Gernaey, K. V., Ashokkumar, S., & Adler-Nissen, J. (2011). Modelling of coupled heat and mass transfer during a contact baking process. *Journal of Food Engineering*, *106*(3), 228–235.

Golmohammadi, A., & Afkari-Sayyah, A. H. (2013). Long-term storage effects on the physical properties of the potato. *International Journal of Food Properties*, *16*(1), 104–113. https://doi.org/10.1080/10942912.2010.529978

Gratzek, J. P., & Toledo, R. T. (1993). Solid Food Thermal Conductivity Determination at High Temperatures. *Journal of Food Science,* 58(4), 908-913

Haak, L., Sioen, I., Raes, K., Camp, J. Van, & Smet, S. De. (2007). Effect of pan-frying in different culinary fats on the fatty acid profile of pork. *Food Chemistry*, *102*(3), 857–864.

624 Houšová, J., & Topinka, P. (1985). Heat transfer during contact cooking of minced meat patties.
625 *Journal of Food Engineering*, *4*(3), 169–188.

626 Huang, L. (2012). A simplified method for numerical simulation of gas grilling of non-intact
627 beef steaks to eliminate Escherichia coli O157:H7. *Journal of Food Engineering*, *113*(3),
628 380–388.

629 Incropera, F.P., DeWitt, D.P., Bergman, T., & Lavine A. (2007). Fundamentals of Heat and
630 Mass Transfer, sixth ed. John Wiley and Sons.

631 Madhusudana, C.V. (1996). Introduction. In *Thermal Contact Conductance*. New York, NY:
632 Springer-Verlag New York, Inc.

633 Ou, D., & Mittal, G. S. (2006). Double-sided pan-frying of unfrozen/frozen hamburgers for
634 microbial safety using modelling and simulation. *Food Research International*, *39*(2),
635 133–144.

636 Pan, Z., & Singh, R. P. (2002). Heating Surface Temperature and Contact-Heat Transfer
637 Coefficient of a Clam-Shell Grill. *LWT - Food Science and Technology*, *35*(4), 348–354.

638 Rocca-Poliméni, R., Zárate Vilet, N., Roux, S., Bailleul, J.-L., & Broyart, B. (2019).
639 Continuous measurement of contact heat flux during minced meat grilling. *Journal of*
640 *Food Engineering*, *242*, 163–171.

641 Ronald, T., Magee, A., Wilkinson, P.D. (1992), Influence of Process Variables on the Drying

642 of Potato Slices, Int. 1. Heat and Mass Transfer, 27 p. 541-549.

643 Sanz-Serrano, F., Sagues, C., Feyissa, A. H., Adler-Nissen, J., & Llorente, S. (2017). Modeling
644 of pancake frying with non-uniform heating source applied to domestic cookers. *Journal*
645 *of Food Engineering*, *195*, 114–127.

646 Sioen, I., Haak, L., Raes, K., Hermans, C., De Henauw, S., De Smet, S., & Van Camp, J. (2006).
647 Effects of pan-frying in margarine and olive oil on the fatty acid composition of cod and
648 salmon. *Food Chemistry*, *98*(4), 609–617.

649 Wang, N., & Brennan, J. G. (1991). Moisture sorption isotherm characteristics of potatoes at
650 four temperatures. *Journal of Food Engineering*, *14*(4), 269–287.
651 https://doi.org/10.1016/0260-8774(91)90018-N

652 Wang, N., & Brennan, J. G. (1993). The influence of moisture content and temperature on the
653 specific heat of potato measured by differential scanning calorimetry. *Journal of Food*
654 *Engineering*, *19*(3), 303–310. https://doi.org/10.1016/0260-8774(93)90049-P

655 Wichchukit, S., Zorrilla, S. E., & Singh, R. P. (2001). Contact heat transfer coefficient during
656 double-sided cooking of hamburger patties. *Journal of Food Processing and Preservation*,
657 *25*(3), 207–221.

658 Zorrilla, S. E., & Singh, R. P. (2000). Heat Transfer in Meat Patties during Double-Sided
659 Cooking. *Food Science and Technology Research*, *6*(2), 130–135.

660 Zorrilla, S. E., & Singh, R. P. (2003). Heat transfer in double-sided cooking of meat patties
661 considering two-dimensional geometry and radial shrinkage. *Journal of Food*
662 *Engineering*, *57*(1), 57–65.

Figure captions

Fig 1. Laboratory contact heating device.

Fig 2. Schematic representation of the two phases of the model. (a) Stage 1. (b) Stage 2.

Fig 3. Experimental data as a function of heating time for six operating conditions. Mean values (symbols) and standard deviation (error bars) are shown. (a) Heating surface temperature. (b) Water loss. (c) Food product temperature at three locations for experiments with oil. (d) Food product temperature at three locations for experiments without oil.

Fig 4. Comparison between experimental (exp) and simulated (sim) data for a contact heating operation performed at 3.2 $kW.m^{-2}$, with oil and without oil. (a) Water loss. (b) Food product temperature at three locations.

Fig 5. Comparison between experimental (exp) and simulated (sim) data for a contact heating operation performed at 6.4 $kW.m^{-2}$, with oil and without oil. (a) Water loss. (b) Food product temperature at three locations.

Fig 6. Comparison between experimental (exp) and simulated (sim) data for a contact heating operation performed at 9.6 $kW.m^{-2}$, with oil and without oil. (a) Water loss. (b) Food product temperature at three locations.

Fig 7. Temperature distribution (a) and water content distribution (b) in the product calculated by the model for heating at 3.2 $kW.m^{-2}$, with oil.

688

689 **Fig 8.** Thermal contact resistance and thermal resistance of the crust as a function of heating

690 time. (a) Operating conditions with oil. (b) Operating conditions without oil.

691 **Figure 1**

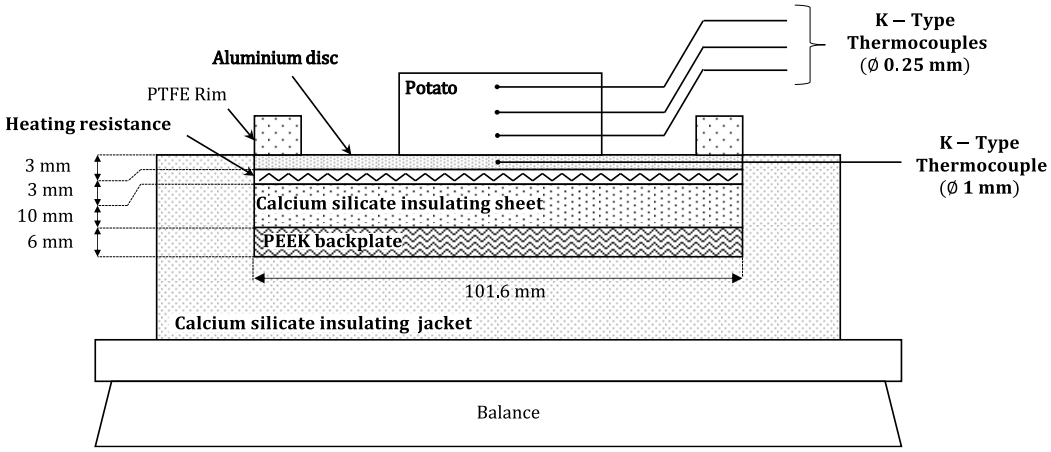

692

693

694 **Figure 2**

695

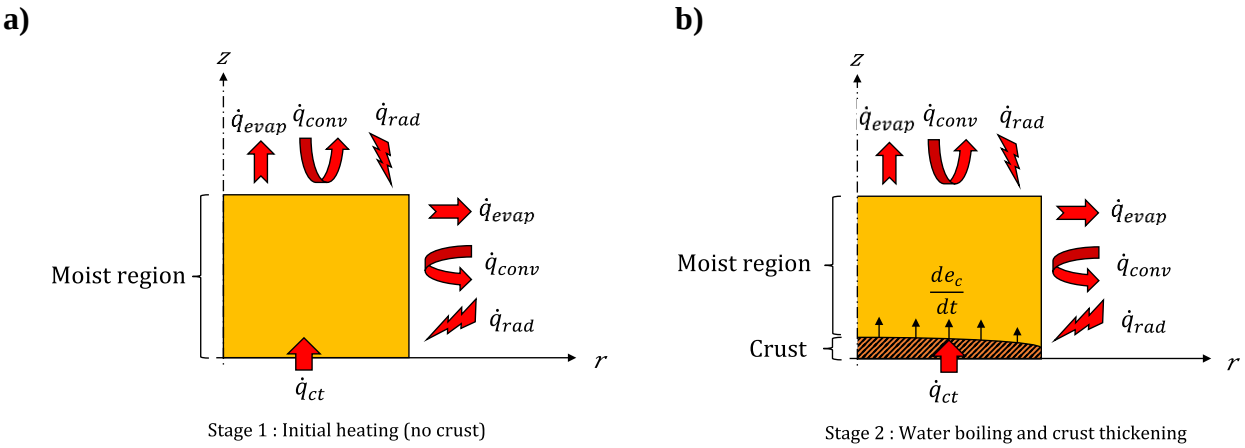

Stage 1 : Initial heating (no crust)

Stage 2 : Water boiling and crust thickening

Figure 3

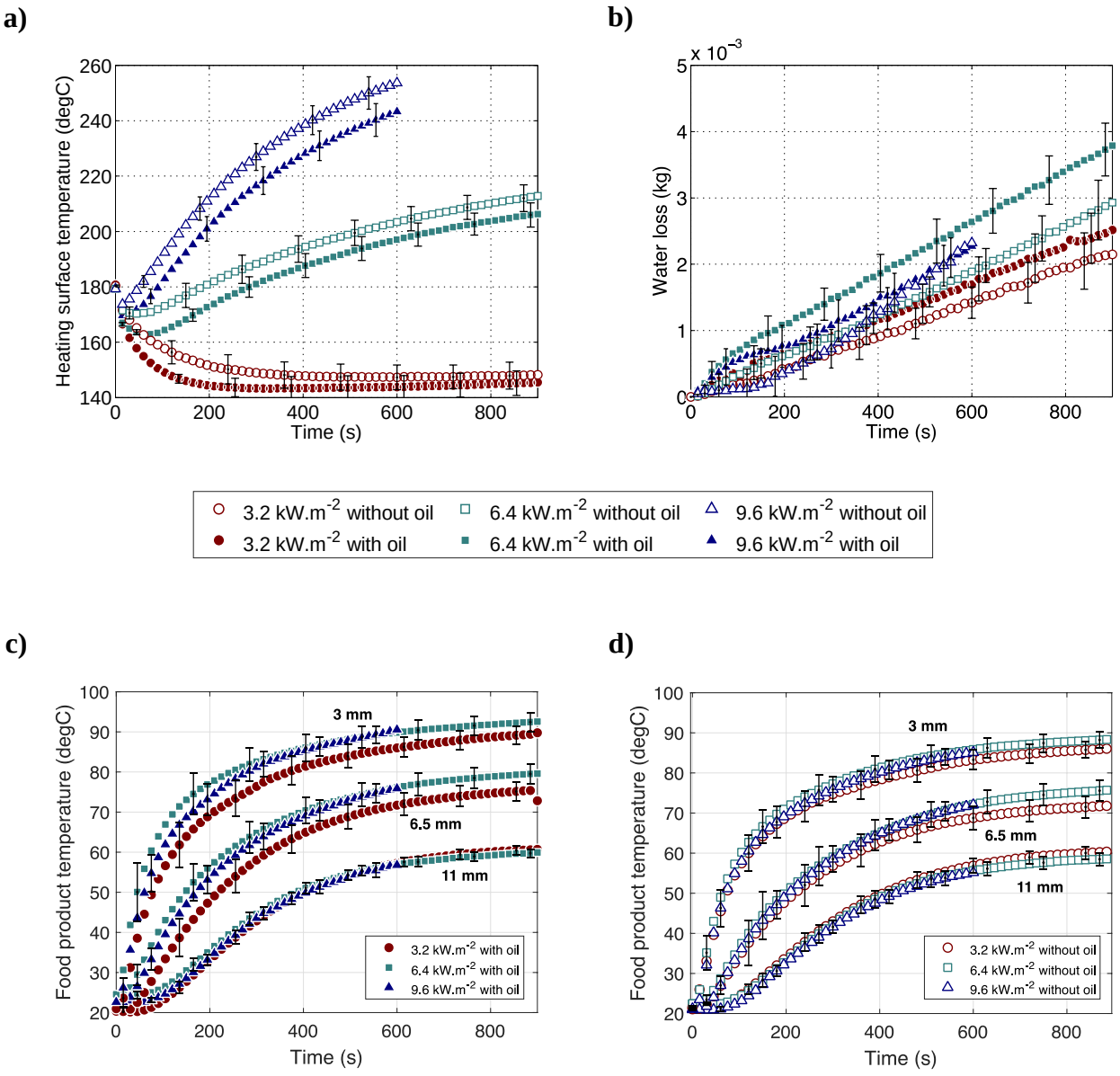
a)
b)
Heating surface temperature (degC)
Time (s)
x 10^-3
Water loss (kg)
3.2 kW.m-2 without oil
6.4 kW.m-2 without oil
9.6 kW.m-2 without oil
3.2 kW.m-2 with oil
6.4 kW.m-2 with oil
9.6 kW.m-2 with oil
c)
d)
Food product temperature (degC)
3 mm
6.5 mm
11 mm

Figure 4

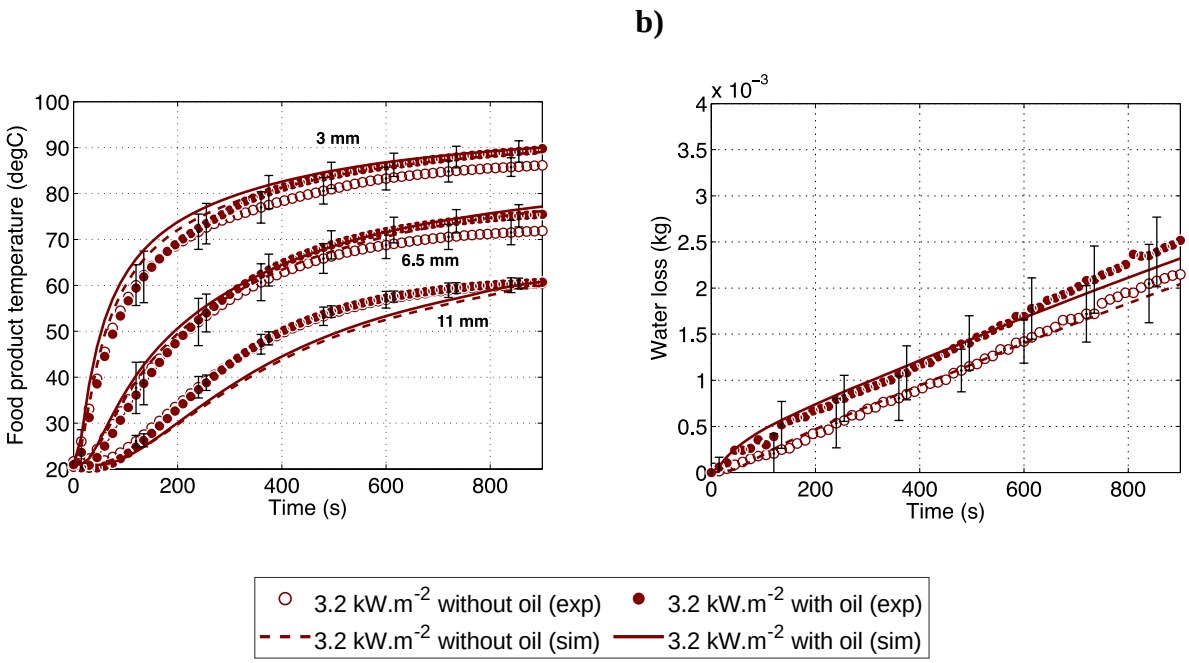

Figure 5

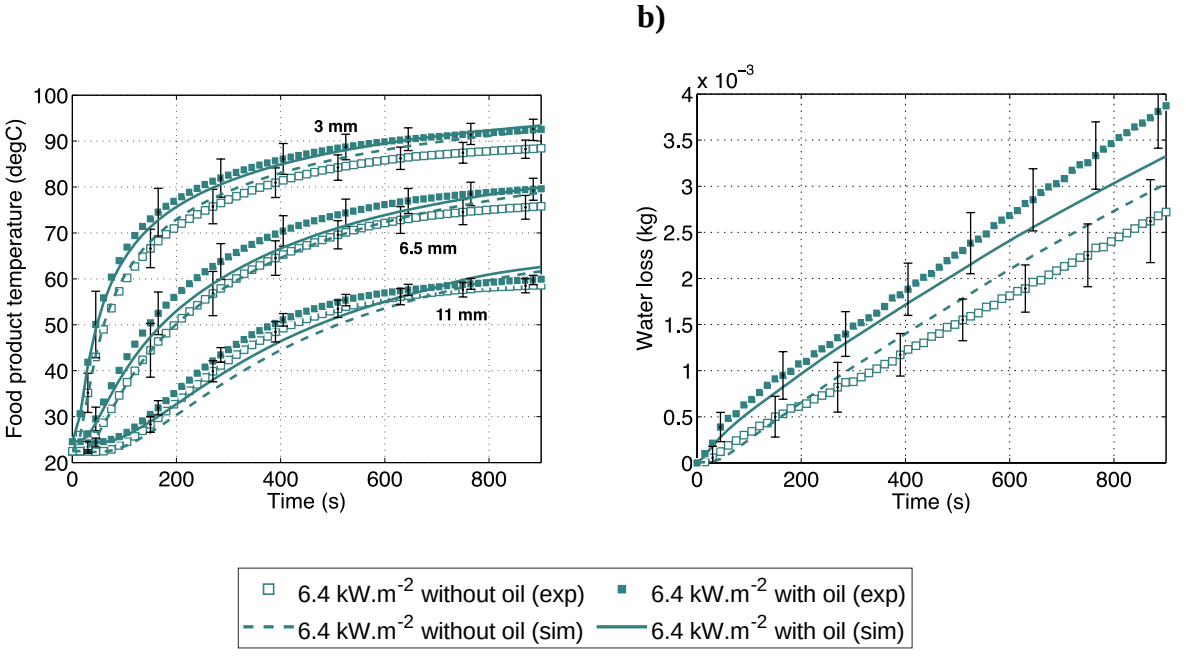

Figure 6

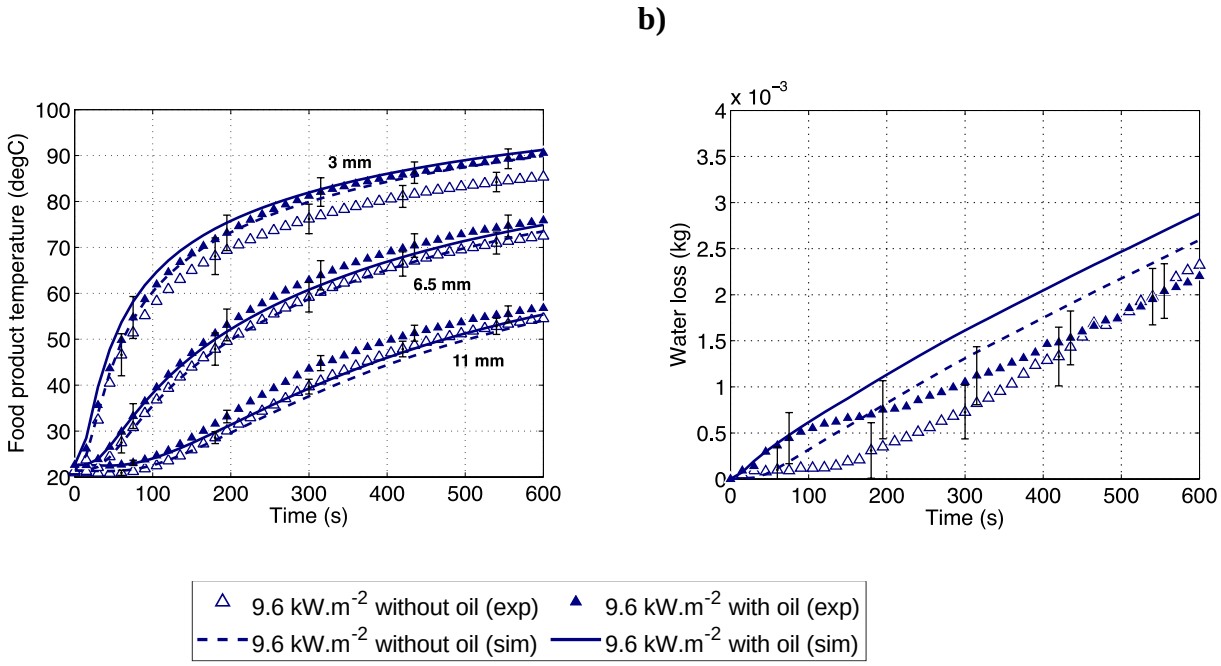

Figure 7

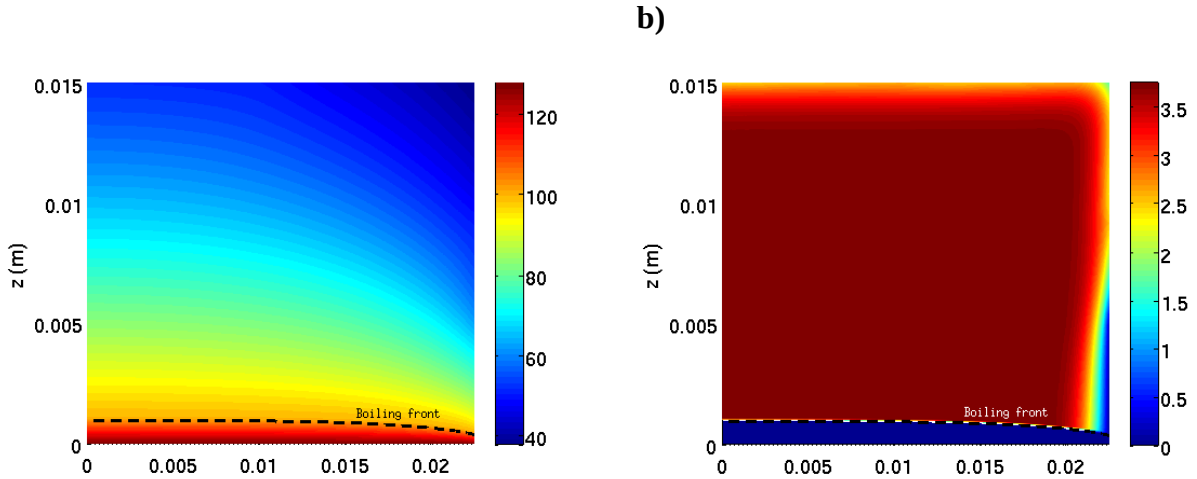

727 **Figure 8**

728

a)

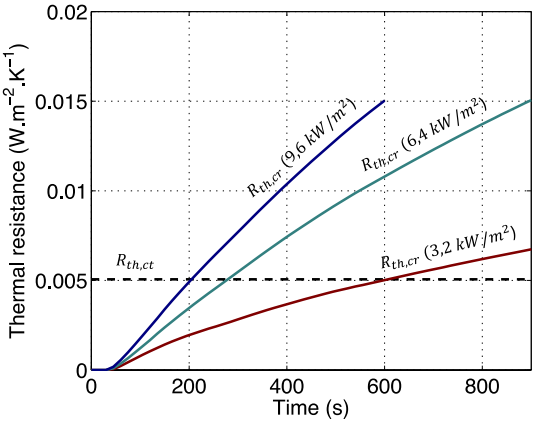

b)

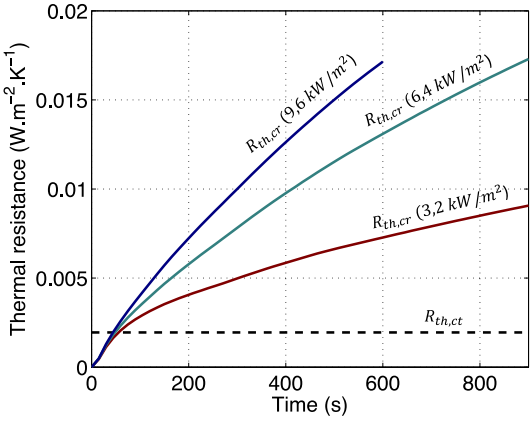

729 **Table 1.** Comparison between sensible heat and latent heat consumed in the product calculated
730 by the model for each operating condition at 600 s of heating.
731

	With oil			Without oil		
	3.2 kW.m^{-2}	6.4 kW.m^{-2}	9.6 kW.m^{-2}	3.2 kW.m^{-2}	6.4 kW.m^{-2}	9.6 kW.m^{-2}
E_{sens}	3808 J	3727 J	3662 J	3777 J	3711 J	3658 J
E_{vapo}	4080 J	5763 J	6978 J	3331 J	5006 J	6210 J

732